Ion-Selective Electrodes with Colloid-Imprinted Mesoporous Carbon as Solid Contact

ARTICLE *in* ANALYTICAL CHEMISTRY · JULY 2014

Impact Factor: 5.64 · DOI: 10.1021/ac501633r · Source: PubMed

4 AUTHORS, INCLUDING:

Philippe Buhlmann
University of Minnesota Twin Cities
155 PUBLICATIONS **7,950** CITATIONS

SEE PROFILE

analytical chemistry

Article

pubs.acs.org/ac

Ion-Selective Electrodes with Colloid-Imprinted Mesoporous Carbon as Solid Contact

Jinbo Hu, Xu U. Zou, Andreas Stein,* and Philippe Bühlmann*

Department of Chemistry, University of Minnesota, 207 Pleasant St. SE, Minneapolis, Minnesota 55455, United States

Supporting Information

ABSTRACT: A new type of solid-contact ion-selective electrode (SC-ISE) has been developed that uses colloid-imprinted mesoporous (CIM) carbon with 24 nm diameter, interconnected mesopores as the intermediate layer between a gold electrode and an ionophore-doped ISE membrane. For a demonstration, valinomycin was used as K^+ ionophore, and a good Nernstian response with a slope of 59.5 mV/decade in the range from $10^{-5.2}$ to $10^{-1.0}$ M was observed. The high purity, low content of redox-active surface functional groups and intrinsic hydrophobic characteristics of CIM carbon prepared from mesophase pitch lead to outstanding performance of these sensors, with excellent resistance to the formation of a water layer and no interference caused by light, O_2, and CO_2. When a redox couple is introduced as an internal reference species, calibration-free SC-ISEs can be made with a standard deviation of E° as low as 0.7 mV. Moreover, the interconnected mesopore structure of ISE membrane-infused CIM carbon facilitates both ion and electron conduction and provides a large interfacial area with good ion-to-electron transduction. Because of the large double layer capacitance of CIM carbon, CIM carbon-based SC-ISEs exhibit excellent potential stability, as shown by chronopotentiometry and continuous potentiometric measurements. The capacitance of these electrodes as determined by chronopotentiometry is 1.0 mF, and the emf drift over 70 h is as low as 1.3 μV/h, making these electrodes the most stable SC-ISEs reported so far.

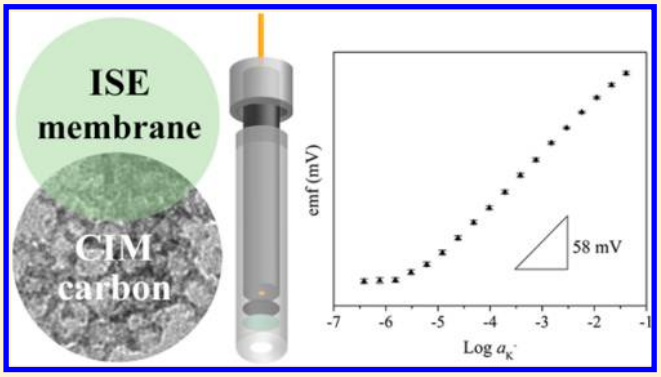

Ion-selective electrodes (ISEs) are widely used in various application fields, including clinical analysis, process control, and environmental monitoring.[1−5] To achieve sensor miniaturization, small sample volumes, easy maintenance, and scalability for mass production, solid-contact ion-selective electrodes (SC-ISEs), in which a solid contact is used as the ion-to-electron transducer, have attracted much attention.[3,6−8]

The first proposed SC-ISE, the coated-wire electrode, was extremely simple but unreliable due to the ill-defined interfacial potential between the ion-selective membrane (ISM) and the underlying conducting metal.[9] To stabilize this interfacial potential, intermediate layers consisting of conducting polymers with high redox capacitance, such as derivatives of polypyrrole,[10] polythiophene,[11] and polyaniline,[12] were introduced. Some of these sensors have shown interference from gases[13] or are affected by the buildup of an unintended water layer between the ISM and the solid contact.[14] More importantly, conducting polymer films do not have a well-defined redox potential but instead exhibit a continuum of redox potentials (which manifests itself, e.g., by broad, scan rate independent peaks in cyclic voltammograms).[15] There are several causes for this energetic inhomogeneity, including the coexistence of crystalline and amorphous regions,[16] slow conformational changes as the result of oxidation or reduction (often referred to as redox transformations, the slowness of which manifests itself in hysteresis),[17,18] changes in the glass transition temperature as a result of doping,[19] the formation of intermolecular bonds between neighboring chains,[15] and the dependence of the film morphology on the method of film fabrication.[20,21] Moreover, the penetrability of counterions and, concomitantly, the film capacitance depend on the counterion size[22] and, likely, the local polymer morphology. Consequently, it is difficult to obtain high device-to-device reproducibility and to minimize long-term drift resulting from reactions of the conducting polymer with ambient redox-active species such as oxygen.

More recently, nanostructured carbon materials such as three-dimensionally ordered macroporous (3DOM) carbon,[23,24] carbon nanotubes,[25,26] fullerene,[27] and graphene[28−30] have gained the attention of electrochemists due to their intrinsic hydrophobicity and electric conductivity. SC-ISEs based on these carbon materials have exhibited few problems with water layer formation and interference by O_2, CO_2, or light. Among the sensors with one of these carbon materials as an interlayer, the 3DOM carbon-based SC-ISEs have shown the most favorable long-term potential stability,

Received: May 4, 2014
Accepted: June 18, 2014
Published: July 1, 2014

   dx.doi.org/10.1021/ac501633r | *Anal. Chem.* 2014, 86, 7111−7118

which can be explained by the high capacitance of the interface between this carbon material and the ISM.

3DOM carbon consists of a glassy carbon skeleton with interconnected macropores that can be infiltrated with the ISM to form a bicontinuous structure, in which electrons are conducted through the carbon framework while ions move through the infused ISM. Its large interfacial contact area and high capacitance lead to excellent long-term stability of 3DOM carbon-based SC-ISEs, with a drift as low as 11.7 μV/h.[23,24] With these sensors, a subnanomolar detection limit of Ag^{+}[31] and trace-level detection of perfluorinated surfactants in lake water[32] have been achieved. However, 3DOM carbon prepared from resorcinol−formaldehyde precursors contains significant amounts of redox-active surface functional groups[24] that can affect the reproducibility of the calibration curve intercept, E^{o}. As a consequence, SC-ISEs that use 3DOM carbon still require calibration. Moreover, the monolithic nature of 3DOM carbon as used in the past is problematic in view of mass production of sensors.

To address issues of E^{o} reproducibility and with the ultimate goal to prepare calibration-free SC-ISEs, we report here the investigation of colloid-imprinted mesoporous (CIM) carbon as a new solid contact material. Similar to 3DOM carbon, CIM carbon exhibits open and interconnected pores that can form a bicontinuous carbon and pore space. It can be synthesized by employing a colloidal imprinting method, in which colloidal silica is used as the template and mesophase pitch as the carbon precursor.[33] Both of these starting materials are inexpensive and commercially available, and the synthesis can be easily scaled up. The mesopore size and pore volume of CIM carbon can be tuned by the size of the colloidal silica particles, usually ranging from approximately 10 to 50 nm depending on the source of colloidal silica.[34] Due to its pore texture, CIM carbon exhibits a higher capacitance than 3DOM carbon. In addition, the high purity carbon precursor for CIM carbon, i.e., the mesophase pitch, introduces fewer redox-active surface functional groups. While pitch materials obtained from coal tar or petroleum products have mixed compositions and are difficult to purify, the type of mesophase pitch used here as precursor for the preparation of CIM carbon is a fully synthetic material prepared by condensation of an aromatic hydrocarbon, accounting for its exceptional purity and low oxygen content.[35] Moreover, unlike monolithic 3DOM carbon, CIM carbon is prepared in powder form and can be made into thin films for mass production and fabrication. CIM carbon has been used as a template for zeolite synthesis[36] and as a stationary phase for reversed-phase liquid chromatography,[37] but its utilization as a solid contact material for ISEs is novel.

Herein, we report the use of CIM carbon with 24 nm diameter mesopores as a new solid contact material. Benefiting from the aforementioned characteristics, CIM carbon-based SC-ISEs exhibit excellent Nernstian responses and potential stability. No water layer or interferences by light, O_2, or CO_2 are observed. When combined with a redox buffer layer provided by the tetrakis(pentafluorophenyl)borate ($TPFPB^{-}$) salts of cobalt(II) and cobalt(III) tris(4,4′-dinonyl-2,2′-bipyridyl) ($[Co(dibpy)_3]^{2+/3+}$),[38] SC-ISEs can be fabricated with a standard deviation of E° as low as 0.7 mV. This suggests that for many applications these sensors can be used without prior calibration.

EXPERIMENTAL SECTION

Materials. Reagents were obtained from the following sources: mesophase pitch from Mitsubishi Gas Chemicals (Tokyo, Japan); Ludox AS-40 colloidal silica, sodium ethoxide solution (21 wt % in ethanol), bromocresol green/methyl red (mixed indicator solution in methanol), tetraethylammonium tetrafluoroborate ($TEABF_4$), and valinomycin from Sigma-Aldrich (St. Louis, MO); *o*-nitrophenyl octyl ether (*o*-NPOE) and high molecular weight poly(vinyl chloride) (PVC) from Fluka (Buchs, Switzerland); sodium tetrakis[3,5-bis-(trifluoromethyl)phenyl]borate (NaTFPB) from Dojindo (Kumamoto, Japan); and lithium tetrakis(pentafluorophenyl)-borate (LiTPFPB) ethyl etherate from Boulder Scientific (Boulder, CO). All chemicals were used as received without further purification. Deionized water was purified to a resistivity of 18.2 MΩ/cm with a Milli-Q PLUS reagent-grade water system (Millipore, Bedford, MA). The redox couple consisting of $[Co(dibpy)_3](TPFPB)_2$ and $[Co(dibpy)_3](TPFPB)_3$ was synthesized as reported.[38]

CIM Carbon Synthesis. The CIM carbon was synthesized using a modification of a previously reported route.[33] A mass of 5 g of mesophase pitch was manually ground and dispersed in 100 mL of an ethanol/water mixture (∼60:40 volume ratio) at 50 °C. Under vigorous stirring, 100 mL of Ludox AS-40 colloidal silica suspension was added gradually into the flask, and the resulting mixture was stirred overnight at 50 °C. The resulting mixture was transferred to an open plastic beaker, stirred, and kept at 50 °C overnight to allow solvent evaporation. The obtained pitch−silica composites were then transferred into a porcelain combustion boat and heated under a N_2 flow (0.5 L/min) with a heating ramp of 5 °C/min to 400 °C, at which temperature it was kept for 2 h. The subsequent carbonization at 900 °C for 2 h in a N_2 atmosphere converted the pitch−silica composites to carbon−silica composites. To remove the silica spheres, the carbon−silica composites were then soaked in 6 M KOH aqueous solution and kept for 48 h at 180 °C in a Teflon-lined steel autoclave. The obtained CIM carbon was filtered and washed with copious amounts of water until the pH was 7. Before use, the CIM carbon was pyrolyzed under a 5% H_2, 95% N_2 flow (0.6 L/min) at 900 °C for 5 h to reduce absorbed moisture and functional groups on the carbon surface with preservation of mesopores.[39]

Electrode Fabrication. The 2 mm diameter gold disk electrodes (gold disks embedded into a cylindrical plastic body, CH Instruments, Austin, TX) were polished over polishing cloths with aqueous dispersions of alumina (0.3 and 0.05 μm, Buehler, Lake Bluff, IL). They were cleaned by ultrasonication in water and ethanol and dried with a flow of argon. CIM carbon powder was manually ground for 5 min. The CIM carbon suspension was prepared by ultrasonicating 47.5 mg of CIM carbon and 2.5 mg of PVC as binder in 1 mL of freshly distilled tetrahydrofuran (THF) for 30 min. An amount of 30 μL of the CIM carbon suspension was dropcast onto gold electrodes and left to dry, forming CIM carbon films with a thickness of approximately 200 μm.

Precursor solutions for valinomycin-doped K^{+}-ISMs were prepared by dissolving in 1 mL of freshly distilled THF, 66 mg of PVC as polymer matrix, 132 mg of *o*-NPOE as plasticizer, 2.0 mg of valinomycin as ionophore, and 1.2 mg of NaTFPB (75 mol % with respect to the ionophore) to provide for ionic sites. Solutions for K^{+}-ISMs doped with the redox couple were prepared by dissolving in 1 mL of freshly distilled THF, 66 mg

dx.doi.org/10.1021/ac501633r | Anal. Chem. 2014, 86, 7111−7118

of PVC, 132 mg of *o*-NPOE, 2.0 mg of valinomycin, 0.6 mg of LiTPFPB ethyl etherate (46 mol % with respect to the ionophore) to provide for anionic sites, and 1.4 mmol/kg each of $[Co(dibpy)_3](TPFPB)_2$ and $[Co(dibpy)_3](TPFPB)_3$.

To form ISMs with a thickness of approximately 100 μm, two portions of one of the above solutions (20 μL, followed by 30 μL) were dropcast onto the CIM carbon layer on a gold disk electrode. As a precaution to avoid the possible delamination of the ISMs and CIM carbon films from the gold electrodes, the coated electrodes were mounted into cylindrical bodies custom-made from the Dupont Delrin acetal resin. A screw cap at the opposite end of the electrode allowed one to gently press the ISM with the CIM carbon film onto the electrode (see Figure 1 and Supporting Information Figure S1). (Use of gold disk electrodes embedded into or printed onto a PVC compatible polymer, rather than the commercial gold disk electrodes as used here, would make the cylindrical bodies unnecessary.) Prior to measurements, the electrodes with the redox couple were conditioned in 1.0 mM KCl solution for 1 h, and those without the redox couple for 24 h. The short conditioning time of the electrode membranes containing the redox couple minimized the loss of redox couple species by leaching into the aqueous solution, as discussed in ref 38.

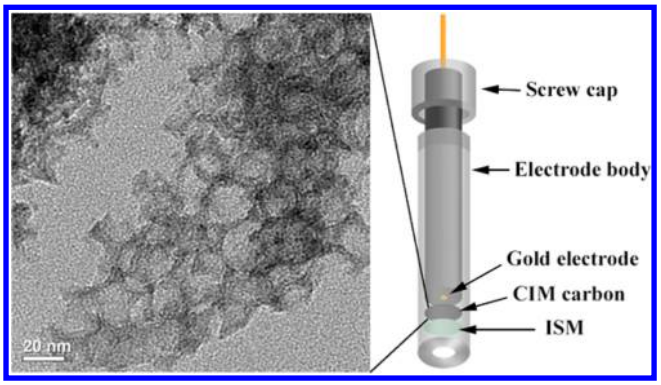

Figure 1. Schematic diagram of a CIM carbon-based SC-ISE with a TEM image showing the interconnected mesopores of CIM carbon. CIM carbon is used as an intermediate layer between the gold electrode and ISM.

CIM Carbon Characterization. Acid–base titrations to determine surface functional groups were performed according to a previously reported procedure.[24,40] C, H, and N elemental analyses were performed by Atlantic Microlab (Norcross, GA). Transmission electron microscopy (TEM) was carried out with a Technai T12 microscope (FEI, Hillsboro, OR) operating at 120 kV with emission currents ranging from 7 to 12 μA. Nitrogen-sorption measurements were performed on an Autosorb iQ_2 gas sorption analyzer (Quantachrome, Boynton Beach, FL), with samples outgassed at 1 mTorr at 200 °C for 12 h before measurements. Specific surface areas were calculated by the Brunauer–Emmett–Teller (BET) method, and the pore sizes and volumes were estimated from the pore size distribution curves obtained from the adsorption branches of the isotherms using the Barrett–Joyner–Halenda (BJH) method.

Potentiometric Measurements. Electrode potentials were measured with an EMF 16 potentiometer (input impedance 10 TΩ) controlled by EMF Suite 1.03 software (Lawson Labs, Malvern, PA). A double-junction type external reference electrode (DX200, Mettler Toledo, Switzerland; 3.0 M KCl saturated with AgCl as inner filling solution and 1.0 M LiOAc as bridge electrolyte) was used. Activity coefficients were calculated according to a two-parameter Debye–Hückel approximation,[41] and all emf values were corrected for liquid-junction potentials with the Henderson equation.[42]

Capacitance Measurements. A three-electrode setup was used for measurements of the capacitance of CIM carbon. A gold electrode with a CIM carbon film was used as the working electrode, a Pt wire as the counter electrode, and a Ag wire in $AgNO_3$/acetonitrile as a nonaqueous reference electrode. To ensure complete wetting of CIM carbon, 0.1 M $TEABF_4$ in propylene carbonate was used as the nonaqueous electrolyte. The electrolyte solution was purged with argon for 15 min prior to each measurement.

For cyclic voltammetry experiments, a potential window of 0.6 V centered at 0.0 V with a scan rate of 0.5 mV/s was used. The capacitance was calculated by averaging the absolute value of the two current values at 0.0 V. This average current was then divided by the scan rate and the mass of the CIM carbon to give a specific capacitance value in F/g.

Electrochemical impedance spectroscopy (EIS) experiments were carried out on a Solartron 1255B frequency response analyzer with an SI 1287 electrochemical interface (Farnborough, Hampshire, U.K.) controlled by ZPlot software, and the data was fit using ZView software (Scribner Associates, Southern Pines, NC). The frequency range was 1 MHz to 0.01 Hz, with an ac amplitude of 10 mV versus the open circuit potential.

For chronopotentiometry experiments involving a CIM carbon film on a gold electrode, a constant current of 0.1 mA was applied to the working electrode until an upper potential limit of 1.0 V was reached, at which time an equal but opposite current was applied to discharge the device until a lower potential limit of 0.0 V was reached. The specific capacitance in F/g was calculated by dividing the applied current by the mass of the CIM carbon and by the slope of the discharge curve in a potential versus time graph.

For chronopotentiometry measurements with CIM carbon-based ISEs, a gold electrode coated with CIM carbon and an ISM without a redox couple was used as the working electrode, a 1 mM KCl solution was used as aqueous electrolyte, and an aqueous double-junction Ag/AgCl electrode (with a 1.0 M LiOAc bridge electrolyte and AgCl-saturated 3.0 M KCl inner reference electrolyte) and a Pt wire served as the reference and counter electrodes, respectively. A constant current of +1 nA was applied to the ISE for 60 s, followed by a reverse current of the same magnitude for the same length of time.[43] The capacitance of the electrode was calculated by using the constant current divided by the slope of the discharge curve in a potential versus time graph.

RESULTS AND DISCUSSION

Structure of CIM Carbon. The CIM carbon prepared in this work has remarkably uniform mesopores of about 24 nm (Supporting Information Figure S2) due to the monodispersity of the colloidal silica particles that were used to template the pores.[33] As Figure 1 shows, these mesopores are highly interconnected but randomly distributed, which is different from the periodic nature of 3DOM carbon. After manual grinding for 5 min, CIM carbon particles have irregular shapes with average sizes of approximately 15 μm. When used in a SC-ISE, these particles are bound together by the PVC binder as well as the plasticized ISM.

dx.doi.org/10.1021/ac501633r | *Anal. Chem.* 2014, 86, 7111–7118

Purity and Surface Functionality of CIM Carbon. CIM carbon exhibits higher purity and fewer surface functional groups than 3DOM carbon because its carbon precursor, the mesophase pitch used here, is a polyaromatic resin produced by catalytic synthesis from naphthalene, comprising only carbon and hydrogen.[35] In comparison, the resorcinol–formaldehyde precursor of 3DOM carbon contains a considerable amount of oxygen, which can introduce oxygen-based impurities. As shown in Table 1, the oxygen content of CIM carbon is 0.43 wt %, i.e., 1.7 wt % lower than that of 3DOM carbon synthesized from resorcinol–formaldehyde. The surface functionality of CIM carbon was characterized by acid–base titrations with four different bases, as previously reported.[24,40] In contrast to 3DOM carbon (see Table 2), no phenol functional groups are detected, and the ketone content is cut in half. We assume that the residual trace amount of oxygen in CIM carbon arises from the KOH hydrothermal treatment used to remove the silica template as well as from small amounts of unremoved silica.

Table 1. Elemental Analysis Data for CIM Carbon and 3DOM Carbon[a]

	C (wt %)	H (wt %)	O (wt %)	N (wt %)
CIM carbon	96.02	0.46	0.43	0.00
3DOM carbon[24]	92.95	0.27	2.13	0.00

[a]All elemental analysis values are ±0.3% according to Atlantic Microlab.

Table 2. Concentration of Functional Groups on the Surface of CIM Carbon and 3DOM Carbon

	ketone (mmol/g)	phenol (mmol/g)	lactone and lactol (mmol/g)	carboxylic acid[a] (mmol/g)
CIM carbon	0.17	0.00	0.00	0.00
3DOM carbon[24]	0.34	0.27	0.00	0.00

[a]The titration method cannot distinguish between carboxylic acid and anhydride functional groups, which may also be present.

Capacitance of CIM Carbon. Mesoporous carbon materials are well-known for their high double layer capacitance due to their large surface areas and highly accessible mesopores.[44] In this study, three electrochemical techniques, i.e., cyclic voltammetry (CV), chronopotentiometry, and electrochemical impedance spectroscopy (EIS), were used to determine the specific capacitance of the CIM carbon. For all the measurements, a gold electrode with a CIM carbon film was used as the working electrode, with 0.1 M $TEABF_4$ in propylene carbonate as the electrolyte solution that effectively wets CIM carbon.

In the CV measurement obtained with a scan rate of 0.5 mV/s, a symmetrical curve without Faradaic currents, typical for capacitive behavior, is observed (Figure 2A). The absence of Faradaic currents demonstrates the low amount of redox-active surface functional groups on the CIM carbon. For chronopotentiometry, a constant current of +0.1 mA was applied to the working electrode until the potential reached +1.0 V, and then, a current of −0.1 mA was applied until the potential reached 0.0 V. Except for the immediate voltage drop after current reversal, the chronopotentiogram appears symmetrical with respect to charging and discharging (Figure 2B). For the EIS data (Figure 2C), the capacitance of CIM carbon can be represented by the impedance of the electrode at low frequencies ranging from 1 to 0.01 Hz. This data can be fitted with a constant phase element (CPE1 in Figure 2C) with a capacitance of 27 mF and a phase value of 0.94, representing capacitive behavior. The specific capacitance of CIM carbon is obtained by dividing the absolute capacitance of the working electrode by the mass of CIM carbon. Those values are summarized and compared with the corresponding values for 3DOM carbon in Table 3. It is very likely that the different

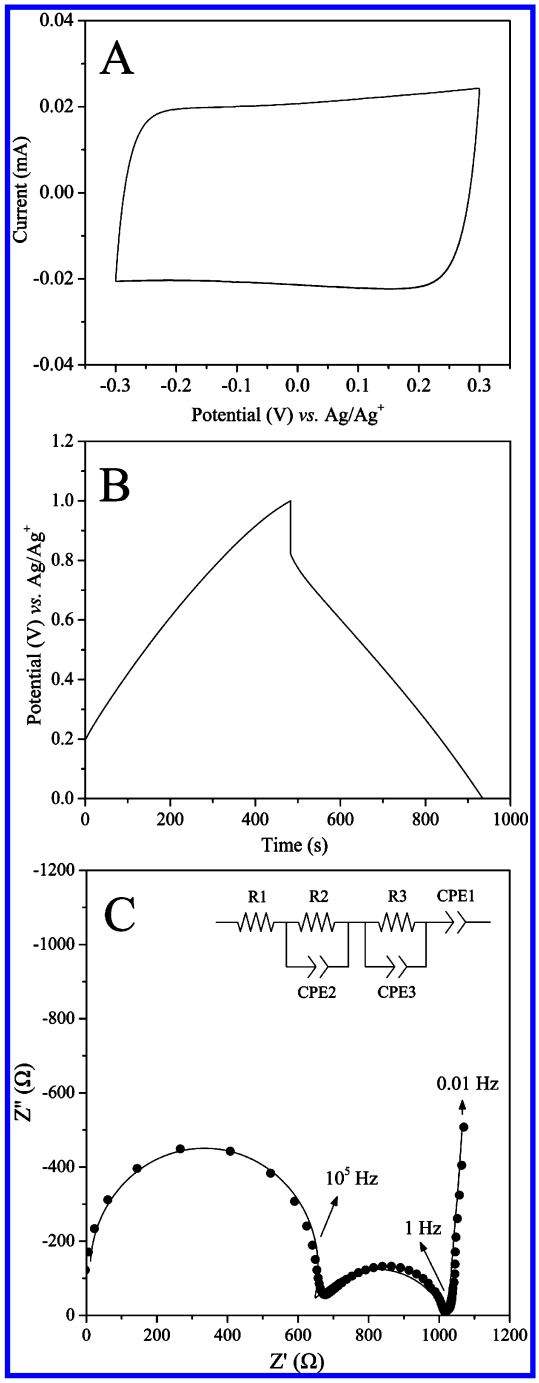

Figure 2. Capacitance measurements of a gold/CIM carbon electrode using 0.1 M $TEABF_4$ as the nonaqueous electrolyte. (A) CV with a scan rate of 0.5 mV/s. (B) Chronopotentiometry with a constant current of 0.1 mA. (C) EIS; the actual data is shown as the solid circles, and the solid line represents the data fit. The proposed equivalent circuit is shown in the inset.

dx.doi.org/10.1021/ac501633r | Anal. Chem. 2014, 86, 7111−7118

Table 3. Specific Capacitance of CIM and 3DOM Carbon as Measured by Different Methods

	CV[a] (F/g)	chrono-potentiometry[b] (F/g)	EIS (F/g)
CIM carbon	31.3	40.7	20.5
3DOM carbon[24]	3.9	2.3	1.8

[a]Scan rate, 0.5 mV/s. [b]Current, 0.1 mA.

values determined with these electrochemical techniques are affected by the different magnitudes of current passing through the working electrode, which can affect the rate of ion transport across the interconnected mesopores of CIM carbon.[45]

Due to the occurrence of redox reactions in the CV and chronopotentiometry experiments for 3DOM carbon,[24] specific capacitance values determined by EIS are more suitable for comparison. This data shows that CIM carbon has a specific capacitance of 20.5 F/g, which is 11 times higher than that for 3DOM carbon. The large capacitance of CIM carbon is due to its interconnected mesopores with average diameters of 24 nm that are accessible to the electrolyte, whereas less accessible micropores, 1.8 nm in average diameter, contribute to most of the surface area of 3DOM carbon (see Supporting Information Table S1). From nitrogen-sorption data (Supporting Information Figure S2), the mesopore surface area of CIM carbon was determined to be 321 m^2/g, which is nearly 13 times that of 3DOM carbon. This ratio is in good agreement with the observed specific capacitance values for these two carbon materials.

Ionic Response. The ionic response of the CIM carbon-based SC-ISEs was measured by successive dilution of a 0.1 M KCl solution while monitoring the emf. For comparison, three different electrode assemblies were used, i.e., a gold electrode with an ISM (gold/ISM), a gold electrode with a CIM carbon intermediate layer and an ISM (gold/CIM carbon/ISM), and a gold electrode with a CIM carbon layer and an ISM doped with the redox couple of $[Co(dibpy)_3](TPFPB)_2$ and $[Co(dibpy)_3](TPFPB)_3$ (gold/CIM carbon/ISM with redox couple). The corresponding calibration curves and other potentiometric K^+ response characteristics of these electrodes are shown in Figure 3 and summarized in Table 4.

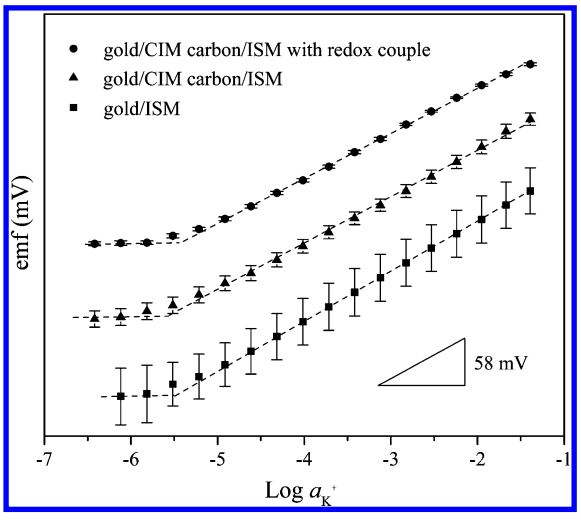

Figure 3. Potentiometric K^+ response curves of SC-ISEs with different electrode configurations, i.e., a gold/CIM carbon/ISM with redox couple, a gold/CIM carbon/ISM, and a gold/ISM electrode. For clarity, response curves have been shifted vertically.

Table 4. Potentiometric K^+ Responses of Different Electrode Assemblies

electrode type	slope (mV/decade)[a]	E° (mV)[a]	detection limit (M)	linear range (M)
gold/CIM carbon/ISM with redox couple	57.3 ± 0.5	237.5 ± 0.7	$10^{-5.4}$	$10^{-5.0}$–$10^{-1.0}$
gold/CIM carbon/ISM	59.5 ± 0.6	58.8 ± 7.3	$10^{-5.6}$	$10^{-5.2}$–$10^{-1.0}$
gold/ISM	64.0 ± 1.4	466.6 ± 32.2	$10^{-5.5}$	$10^{-5.2}$–$10^{-1.0}$

[a]Average and standard deviation of slopes and E° values determined individually for 6 different electrodes of each type of electrode. E° values refer to the potential of the ISE cell obtained by extrapolation of the linear section of the emf response to the K^+ activity of 1.0 M.

Since there is no ion- and electron-conducting intermediate layer for the gold/ISM interface, the corresponding electrodes behaved quite poorly, as expected for coated wire electrodes. The reproducibility of the emf of these electrodes can be represented by the standard deviation of E°, which is as large as 32.2 mV due to the ill-defined interfacial potential. The slightly larger than Nernstian slope of 64.0 mV/decade is likely an artifact from the instability of E°. When CIM carbon is used as an intermediate layer between the gold electrode and the ISM, a Nernstian response with a slope of 59.5 mV/decade in the range from $10^{-5.2}$ to $10^{-1.0}$ M is observed. This response is consistent with a high stability of the interfacial potential of the solid contact and can be attributed to the ability of the CIM carbon to combine ionic and electronic conduction when the interconnected mesopores are filled with the ionophore-doped solvent polymeric sensing phase. The detection limit of these sensors is $10^{-5.6}$ M and might be further improved by using reagents of higher purity and more dilute conditioning and starting solutions.[31] Since no internal reference is present, the standard deviation of E° of these electrodes is 7.3 mV. The best results were obtained after the introduction of the redox couple as an internal reference standard since the interfacial potential between the CIM carbon and the ISM is well controlled by the redox couple.[38,46] With a standard deviation of E° as low as 0.7 mV, these SC-ISEs may be used for some applications without calibration. We assume that the low amount of redox active impurities on the surface of CIM carbon is of particular importance for the proper functioning of the redox couple so that the interfacial potential between the CIM carbon and the ISM is controlled by the redox couple rather than redox active impurities.

Water Layer Test. The formation of an unintentional thin water layer between the ISM and the solid contact is a common problem for SC-ISEs when these electrodes are exposed to aqueous solutions for long periods of time. The presence of this water layer can be tested with a method proposed by Pretsch et al. and is indicated by a positive potential drift when changing from a primary cation solution to a solution of a (discriminated) interfering cation and a negative potential drift when changing back to the primary cation solution.[14]

In this experiment, the gold/CIM carbon/ISM electrodes were initially conditioned in a 0.1 M KCl solution for 24 h. At t = 1.03 h, the 0.1 M KCl solution was replaced by a 0.1 M NaCl solution, and an immediate potential drop of 176 mV was observed, confirming a high selectivity for K^+ over Na^+. At t = 3.23 h, the return to the 0.1 M KCl solution resulted in an

dx.doi.org/10.1021/ac501633r | Anal. Chem. 2014, 86, 7111−7118

immediate potential increase back to the original value (Figure 4). During these processes, no potential drift was observed,

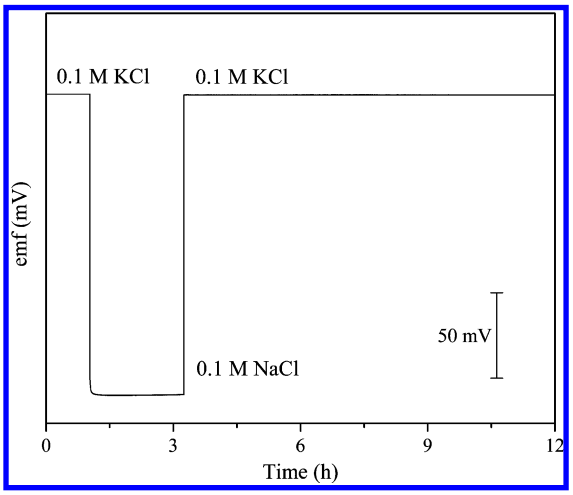

Figure 4. Water layer test for a gold/CIM carbon/ISM electrode. The electrode was immersed in a 0.1 M KCl solution for 24 h prior to the measurement. At t = 1.03 h, the 0.1 M KCl solution was changed to a 0.1 M NaCl solution, and at t = 3.25 h, the 0.1 M NaCl solution was changed back to a 0.1 M KCl solution.

indicating that no water layer had formed in the CIM carbon-based SC-ISEs. The absence of a water layer can be attributed to the highly hydrophobic surface of CIM carbon.

Effects of Light, Oxygen, and Carbon Dioxide. Light, O_2, and CO_2 have been reported to cause interference for several SC-ISEs, especially for SC-ISEs with an interlayer of a conducting polymer.[13] A SC-ISE can be photosensitive if the solid contact is an organic semiconductor with a suitable band gap. In addition, O_2 and CO_2 can diffuse across the ISM to reach the solid contact and cause interference. Specifically, O_2 can affect the phase boundary potential by forming an irreversible O_2 half-cell when redox active species are present, and CO_2 can alter the local pH when a water layer exists between the solid contact and the ISM.[6,47]

In this study, the effect of light on the CIM carbon-based SC-ISEs was investigated by continuously recording the emf of gold/CIM carbon/ISM electrodes in a 1 mM KCl solution while turning on/off the ambient light. Effects of O_2 or CO_2 were tested by bubbling these gases through the solution, followed by purging with Ar to remove O_2 or CO_2. As illustrated in Figure 5, when the sensors were exposed to light, O_2, or CO_2, no significant effect was recorded. The excellent resistance to these interfering agents relies on the low extent of surface functionality and the high hydrophobicity of the surface of CIM carbon.

Potential Stability. The potential stability of gold/CIM carbon/ISM electrodes without redox couple was evaluated by chronopotentiometry[43] by applying consecutively current pulses of +1 nA and −1 nA for 60 s each while recording the potential. For comparison, gold/ISM electrodes without CIM carbon were also tested. As shown in Figure 6, the gold/ISM electrodes are subject to potential drifts up to 0.9 mV/s because of the ill-defined phase boundary potential and low capacitance. When CIM carbon is used as the intermediate layer between the gold electrode and the ISM, the potential drift is significantly reduced to 1.0 ± 0.2 μV/s (n = 3), with an Ohmic drop of 0.36 mV. The capacitance of the electrode is

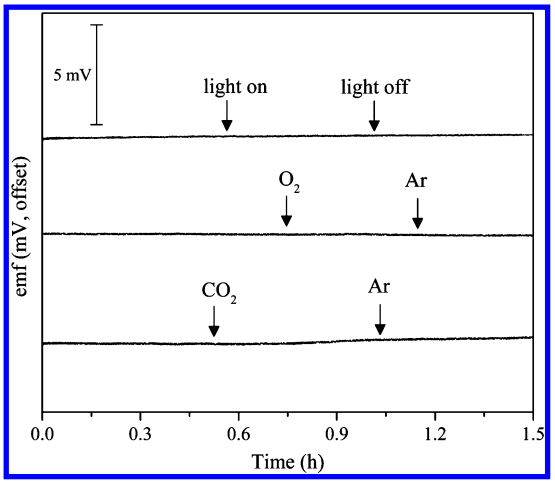

Figure 5. Effects of light (top), O_2 (middle), and CO_2 (bottom) on the potential stability of gold/CIM carbon/ISM electrodes immersed in 1 mM KCl solution. For clarity, the emf responses of these electrodes have been shifted vertically.

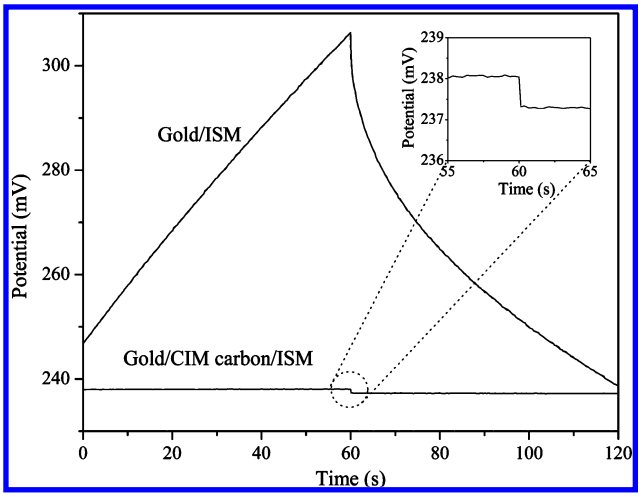

Figure 6. Potential stability of gold/ISM (top) and gold/CIM carbon/ISM (bottom) electrodes under constant currents of ±1 nA in 1 mM KCl solution. An expanded view showing the Ohmic drop of the gold/CIM carbon/ISM electrode at the current reversal point is shown in the inset.

calculated to be 1.0 mF, with a total resistance of 0.36 MΩ. Due to the high double layer capacitance resulting from the interconnected mesopores of CIM carbon, gold/CIM carbon/ISM electrodes exhibit a higher capacitance than other SC-ISEs with valinomycin-doped membranes, such as the electrodes previously studied with interlayers of poly(3,4-ethylenedioxythiophene) (300 μF),[43] carbon black with platinum nanoparticles (217 μF),[48] graphene (83 μF),[30] and carbon nanotubes (60 μF).[25]

Although chronopotentiometry shows on a short time scale a very good potential stability with a relatively large applied current (in comparison to the residual current in potentiometry), other factors such as a gradual decrease in adhesion between the ISM and the substrate[49] might also lead to the deterioration of the electrode response on a longer time scale. Therefore, continuous tests of gold/CIM carbon/ISM electrodes without redox couple were performed for 70 h in 1 mM KCl solution at a constant temperature of 25 °C using temperature-controlled samples. These experiments showed an

dx.doi.org/10.1021/ac501633r | Anal. Chem. 2014, 86, 7111−7118

emf drift of 1.3 ± 0.3 μV/h (n = 3) for gold/CIM carbon/ISM electrodes (Supporting Information Figure S3), making these electrodes the most stable SC-ISEs reported so far. We propose that the high double layer capacitance of CIM carbon contributes to this superior electrochemical performance.

CONCLUSIONS

This work has demonstrated that CIM carbon can be used as a novel solid contact material to construct SC-ISEs. Sensors with a CIM carbon interlayer exhibit good Nernstian responses with excellent resistance to interference by light, O_2, and CO_2 and no indication for the formation of a water layer. Due to the bicontinuous mesopore structure and large double layer capacitance of CIM carbon, outstanding potential stability is achieved under conditions where either a large current is present or continuous potentiometric measurements are conducted. When a redox couple is incorporated into the ISM, SC-ISEs can be constructed with a standard deviation of E° as low as 0.7 mV, which suggests the use for calibration free applications. A challenge for ongoing work lies in the development of even more hydrophobic redox couples that remain in the membrane for very long periods of time. That would then make it possible to perform long-term experiments with ISEs that exhibit the excellent long-term stability of electrodes with CIM carbon solid contacts and the E° reproducibility provided by redox buffers. Compared to other solid contact materials, CIM carbon is cheaper and easier to prepare and process, which makes it more suitable for scale-up than 3DOM carbon. These outstanding characteristics make CIM carbon-based SC-ISEs promising candidates for the next generation of commercial ISEs.

ASSOCIATED CONTENT

Supporting Information

(1) Photograph of a gold electrode mounted into a custom-made electrode body with a screw cap. (2) Nitrogen sorption isotherm and pore size distribution of CIM carbon. (3) Textural data of CIM carbon and 3DOM carbon. (4) Potential stability over 70 h for a gold/CIM carbon/ISM electrode without redox couple. This material is available free of charge via the Internet at http://pubs.acs.org.

AUTHOR INFORMATION

Corresponding Authors

*E-mail: a-stein@umn.edu.
*E-mail: buhlmann@umn.edu.

Notes

The authors declare no competing financial interest.

ACKNOWLEDGMENTS

This research was supported by the University of Minnesota Initiative for Renewable Energy and the Environment (IREE). Portions of this work were carried out in the University of Minnesota Characterization Facility, which receives partial support from the NSF through the MRSEC, ERC, MRI, and NNIN programs. We thank Stephen Rudisill for taking the TEM image of CIM carbon.

REFERENCES

(1) Bakker, E.; Bühlmann, P.; Pretsch, E. *Chem. Rev.* **1997**, *97*, 3083−3132.
(2) Bühlmann, P.; Pretsch, E.; Bakker, E. *Chem. Rev.* **1998**, *98*, 1593−1688.
(3) Bobacka, J.; Ivaska, A.; Lewenstam, A. *Chem. Rev.* **2008**, *108*, 329−351.
(4) Bühlmann, P.; Chen, L. D. In *Supramolecular Chemistry: From Molecules to Nanomaterials*, Jonathan, W., Steed, P. A. G., Eds.; John Wiley & Sons, Ltd: New York, NY, 2012.
(5) Johnson, R. D.; Bachas, L. *Anal. Bioanal. Chem.* **2003**, *376*, 328−341.
(6) Lindner, E.; Gyurcsányi, R. E. *J. Solid State Electrochem.* **2009**, *13*, 51−68.
(7) Michalska, A. *Electroanalysis* **2012**, *24*, 1253−1265.
(8) Pretsch, E. *TrAC, Trends Anal. Chem.* **2007**, *26*, 46−51.
(9) Cattrall, R. W.; Freiser, H. *Anal. Chem.* **1971**, *43*, 1905−1906.
(10) Cadogan, A.; Gao, Z.; Lewenstam, A.; Ivaska, A.; Diamond, D. *Anal. Chem.* **1992**, *64*, 2496−2501.
(11) Bobacka, J.; McCarrick, M.; Lewenstam, A.; Ivaska, A. *Analyst* **1994**, *119*, 1985−1991.
(12) Bobacka, J.; Lindfors, T.; McCarrick, M.; Ivaska, A.; Lewenstam, A. *Anal. Chem.* **1995**, *67*, 3819−3823.
(13) Vázquez, M.; Bobacka, J.; Ivaska, A.; Lewenstam, A. *Sens. Actuators, B* **2002**, *82*, 7−13.
(14) Fibbioli, M.; Morf, W. E.; Badertscher, M.; de Rooij, N. F.; Pretsch, E. *Electroanalysis* **2000**, *12*, 1286−1292.
(15) Vorotyntsev, M. A.; Heinze, J. *Electrochim. Acta* **2001**, *46*, 3309−3324.
(16) Abad, J.; Espinosa, N.; Ferrer, P.; Garcia-Valverde, R.; Miguel, C.; Padilla, J.; Alcolea, A.; Castro, G. R.; Colchero, J.; Urbina, A. *Sol. Energy Mater. Sol. Cells* **2012**, *97*, 109−118.
(17) Egginger, M.; Bauer, S.; Schwödiauer, R.; Neugebauer, H.; Sariciftci, N. S. *Monatsh. Chem.* **2009**, *140*, 735−750.
(18) Csahok, E.; Vieil, E.; Inzelt, G. *J. Electroanal. Chem.* **2000**, *482*, 168−177.
(19) Chen, S.; Ni, J.; Hua, M. *J. Polym. Res.* **1997**, *4*, 261−265.
(20) Kobashi, M.; Takeuchi, H. *Macromolecules* **1998**, *31*, 7273−7278.
(21) Singh, R.; Kumar, J.; Singh, R. K.; Kaur, A.; Sood, K. N.; Rastogi, R. C. *Polymer* **2005**, *46*, 9126−9132.
(22) Veder, J. P.; De Marco, R.; Patel, K.; Si, P.; Grygolowicz-Pawlak, E.; James, M.; Alam, M. T.; Sohail, M.; Lee, J.; Pretsch, E.; Bakker, E. *Anal. Chem.* **2013**, *85*, 10495−10502.
(23) Lai, C.-Z.; Fierke, M. A.; Stein, A.; Bühlmann, P. *Anal. Chem.* **2007**, *79*, 4621−4626.
(24) Fierke, M. A.; Lai, C.-Z.; Bühlmann, P.; Stein, A. *Anal. Chem.* **2010**, *82*, 680−688.
(25) Crespo, G. A.; Macho, S.; Rius, F. X. *Anal. Chem.* **2008**, *80*, 1316−1322.
(26) Crespo, G. A.; Macho, S.; Bobacka, J.; Rius, F. X. *Anal. Chem.* **2008**, *81*, 676−681.
(27) Fouskaki, M.; Chaniotakis, N. *Analyst* **2008**, *133*, 1072−1075.
(28) Ping, J.; Wang, Y.; Wu, J.; Ying, Y. *Electrochem. Commun.* **2011**, *13*, 1529−1532.
(29) Hernández, R.; Riu, J.; Bobacka, J.; Vallés, C.; Jiménez, P.; Benito, A. M.; Maser, W. K.; Rius, F. X. *J. Phys. Chem. C* **2012**, *116*, 22570−22578.
(30) Li, F.; Ye, J.; Zhou, M.; Gan, S.; Zhang, Q.; Han, D.; Niu, L. *Analyst* **2012**, *137*, 618−623.
(31) Lai, C.-Z.; Joyer, M. M.; Fierke, M. A.; Petkovich, N. D.; Stein, A.; Bühlmann, P. *J. Solid State Electrochem.* **2009**, *13*, 123−128.
(32) Chen, L. D.; Lai, C.-Z.; Granda, L. P.; Fierke, M. A.; Mandal, D.; Stein, A.; Gladysz, J. A.; Bühlmann, P. *Anal. Chem.* **2013**, *85*, 7471−7477.
(33) Li, Z.; Jaroniec, M. *J. Am. Chem. Soc.* **2001**, *123*, 9208−9209.
(34) Li, Z.; Jaroniec, M. *Chem. Mater.* **2003**, *15*, 1327−1333.
(35) Mochida, I.; Shimizu, K.; Korai, Y.; Otsuka, H.; Sakai, Y.; Fujiyama, S. *Carbon* **1990**, *28*, 311−319.
(36) Kim, S.-S.; Shah, J.; Pinnavaia, T. J. *Chem. Mater.* **2003**, *15*, 1664−1668.
(37) Li, Z.; Jaroniec, M. *Anal. Chem.* **2004**, *76*, 5479−5485.

(38) Zou, X. U.; Zhen, X. V.; Cheong, J. H.; Bühlmann, P., submitted to *Anal. Chem.*
(39) Li, Z.; Jaroniec, M.; Lee, Y.-J.; Radovic, L. R. *Chem. Commun.* **2002**, 1346−1347.
(40) Boehm, H. P.; Diehl, E.; Heck, W.; Sappok, R. *Angew. Chem., Int. Ed.* **1964**, *3*, 669−677.
(41) Meier, P. C. *Anal. Chim. Acta* **1982**, *136*, 363−368.
(42) Morf, W. E. *The Principles of Ion-Selective Electrodes and of Membrane Transport*; Elsevier: New York, NY, 1981.
(43) Bobacka, J. *Anal. Chem.* **1999**, *71*, 4932−4937.
(44) Nishihara, H.; Kyotani, T. *Adv. Mater.* **2012**, *24*, 4473−4498.
(45) Vu, A.; Li, X.; Phillips, J.; Han, A.; Smyrl, W. H.; Bühlmann, P.; Stein, A. *Chem. Mater.* **2013**, *25*, 4137−4148.
(46) Zou, X. U.; Cheong, J. H.; Taitt, B. J.; Bühlmann, P. *Anal. Chem.* **2013**, *85*, 9350−9355.
(47) Cattrall, R. W.; Drew, D. M.; Hamilton, I. C. *Anal. Chim. Acta* **1975**, *76*, 269−277.
(48) Paczosa-Bator, B.; Cabaj, L.; Piech, R.; Skupień, K. *Anal. Chem.* **2013**, *85*, 10255−10261.
(49) Lindner, E.; Cosofret, V. V.; Ufer, S.; Buck, R. P.; Kusy, R. P.; Ash, R. B.; Nagle, H. T. *J. Chem. Soc., Faraday Trans.* **1993**, *89*, 361−367.